From slow to superluminal propagation: Dispersive properties of surface plasmon polaritons in linear chains of metallic nanospheroids

Alexander A. Govyadinov[1,*] and Vadim A. Markel[2,1,†]

[1]*Department of Bioengineering, University of Pennsylvania, Philadelphia, Pennsylvania 19104, USA*
[2]*Department of Radiology, University of Pennsylvania, Philadelphia, Pennsylvania 19104, USA*
(Received 19 July 2007; revised manuscript received 20 May 2008; published 2 July 2008)

We consider propagation of surface plasmon polaritons (SPPs) in linear periodic chains (LPCs) of prolate and oblate metallic spheroids. We show that the SPP group velocity can be efficiently controlled by varying the aspect ratio of the spheroids. For sufficiently small aspect ratios, a gap appears in the first Brillouin zone of the chain lattice in which propagating modes do not exist. Depending on the SPP polarization, the gap extends to certain intervals of the Bloch wave number q. Thus, for transverse polarization, no propagating SPPs exist with wave numbers q such that $q_c^\perp < |q| < \pi/h$, h being the chain period. For longitudinally polarized SPPs, the gap spans the interval $|q| < q_c^\parallel$. Here $q_c^\perp$ and $q_c^\parallel$ are different constants, which depend on the chain parameters, spheroid aspect ratio, and its orientation with respect to the chain axis. The dependence of the dispersion curves on the spheroid aspect ratio leads to a number of interesting effects. In particular, bandwidth of SPPs that can propagate in an LPC can be substantially increased by utilizing prolate or oblate spheroids. When q is close to a critical value, so that $|q - q_c^\perp| \ll \pi/h$ or $|q - q_c^\parallel| \ll \pi/h$, the decay length of the SPPs is dramatically increased. In addition, the dispersion curves acquire a very large positive or negative slope. This can be used to achieve superluminal group velocity for realistic chain parameters. We demonstrate superluminal propagation of Gaussian wave packets in numerical simulations. Both theory and simulations are based on Maxwell equations with account of retardation and, therefore, are fully relativistic.

I. INTRODUCTION

Propagation of surface plasmon polaritons (SPPs) in linear periodic chains (LPCs) of metal nanoparticles has been in the focus of considerable recent attention.[1–8] The interest is, in part, motivated by the potential application of such chains as subwavelength plasmonic waveguides.[9–11] Since energy in a waveguide can be transported in the form of wave packets, the dispersion relation becomes of primary importance. In the case of LPCs, the dispersion relation is a mathematical dependence of the SPP frequency ω on its Bloch wave number q. It is important to emphasize that the elementary excitations (electromagnetic modes) in LPCs are Bloch waves rather than sinusoidal waves which propagate in continuous media. Only when the Bloch wave number is sufficiently small, so that $qh \ll 1$, where h is the chain period, can we neglect the mathematical distinction between the Bloch and the sinusoidal waves and treat an LPC as an essentially continuous system. How strong the above inequality should be is not evident *a priori*; we will comment on this question in the concluding part of the paper.

Dispersion curves have been previously computed for polarization waves propagating in periodic chains of Drudean spherical nanoparticles.[1–4] It was found that there exist excitations with frequencies ω and Bloch wave numbers q such that $\omega < qc_h$, c_h being the speed of light in the surrounding (host) medium. The phase velocity of such excitations, $v_p = \omega/q$, is less in magnitude than c_h. SPPs with $|v_p| < c_h$ are considered to be outside of the "light cone" and can propagate along the chain without radiative losses, similarly to plane waves in homogeneous dielectrics. We will reserve the term "SPP" specifically for this type of excitations. In a chain of perfectly conducting (lossless) particles, an SPP can propagate infinitely without decay. Of course, absorptive (Ohmic) losses in realistic metals always result in exponential spatial decay of SPPs.

The property of the dispersion curve $\omega(q)$ which is specific to the case of LPCs made of spherical particles is that it is very flat,[1,2,5] with only a weak dependence of the frequency on the Bloch wave number. The dispersion curves are particularly flat for SPPs polarized transversely to the chain. This results in very small group velocities, $v_g \ll c_h$. A factor $v_g/c_h \sim 10^{-2}$ is typical. One practically important consequence of the dispersion curve flatness is a relatively narrow SPP bandwidth. That is, an SPP can be excited in a chain by a spatially localized external source only in a narrow band of frequencies. This can be expected to significantly limit the potential application of LPCs as optical waveguides.

Maier *et al.*[12] have pointed out that the use of spheroidal rather than spherical nanoparticles can result in an increased SPP bandwidth and, correspondingly, in a longer propagation distance. In the above work, the bandwidth was defined as twice the spectral shift of the nearly homogeneous SPP (characterized by $q=0$) with respect to the plasmon peak of an isolated nanoparticle and it was assumed that the propagation distance is proportional to the inverse of the latter. The results were confirmed by FDTD simulations in an LPC of seven prolate nanospheroids whose longer axis was perpendicular to the chain.

In this paper, we further investigate the effects of nonsphericity of the LPC constituents. We compute the dispersion relations in such LPCs in the dipole approximation. We find that the dispersion curves in LPCs are dramatically altered by replacing spherical particles with prolate or oblate spheroids. In particular, the SPP bandwidth can be significantly increased, in agreement with the results of Maier *et al.*

Here, however, we define the bandwidth as the range of frequencies in which efficient SPP transport along the chain is possible. This includes modes with various values of q, including those with $q \sim \pi/h$. We also find that the use of oblate spheroids (nanodisks), whose shorter semiaxis is parallel to the chain, is even more beneficial because it allows one to achieve the desired effect at relatively modest values of the aspect ratio. The increased bandwidth is expected to result in a higher maximum bit rate and longer propagation distances for signals transported by an LPC waveguide.

We further report that, at some critical values of the spheroid aspect ratio, gaps appear in the first Brillouin zone of the lattice. Propagating SPPs do not exist when the Bloch wave number q is inside one of such gaps. When q is near the gap edge, a number of interesting phenomena take place. First, the propagation distance (the decay length) is dramatically increased, as compared to the same quantity when q is far from the edge. Second, the dispersion curves acquire very large positive or negative slopes. In this case, relatively fast $(c_h - |v_g| \ll c_h)$ and even superluminal $(|v_g| > c_h)$ wave packet propagation can be obtained. Note that superluminal group velocity does not contradict special relativity.[13] Superluminal wave packets exist in nature and were observed experimentally.[14,15]

Theory and numerical simulations presented below are based on the dipole approximation. The use of this approximation dictates that the interparticle spacings are larger than a certain threshold at which excitation of higher multipole moments in nanospheroids becomes non-negligible. This has limited the range of chain parameters considered in this paper. We, however, expect on physical grounds that using chains with smaller interparticle separations may be beneficial. For instance, we expect that the SPP propagation length in such chains can be increased. However, in order to obtain quantitative results in that limit, a considerably more complex mathematical formalism must be used. The latter has been developed by Park and Stroud[5] for chains of spherical nanoparticles in the quasistatic limit. Unfortunately, generalization of this formalism to nonspherical particles and beyond the quasistatic approximation (which we deem to be essential for describing SPP propagation in long chains, as was confirmed recently in the experiments by Koenderink *et al.*[16]) appears to be problematic.

The paper is organized as follows: In Sec. II, we describe and justify the basic model used to simulate Bloch waves and wave packets in LPCs. In Sec. III, we compute the dispersion curves for SPPs in chains of prolate and oblate nanospheroids. In Sec. VI, we discuss the attenuation of SPPs due to Ohmic losses in LPCs and, for comparison, in metallic nanowires. In Sec. V, we describe direct numerical simulations of wave packet propagation in LPCs. Sec. IV contains a summary and a discussion of obtained results.

II. BASIC MODEL

Consider a linear periodic chain of identical metallic spheroids with semiaxes a and b ($a \geq b$). We will discuss below two different cases. In the first case, the chain is made of prolate spheroids whose axis of symmetry (which coin-

cides with the longer axis) is perpendicular to the chain. In the second case, the chain is made of oblate spheroids whose axis of symmetry (which coincides with the shorter axis) is parallel to the chain. In both cases, the longer axes of the spheroids are perpendicular to the chain and the eccentricity, e, is given by

$$e = \sqrt{1 - (b/a)^2}. \quad (1)$$

We will refer to the ratio $b/a \leq 1$ of the shorter and longer semiaxes of the spheroids as the aspect ratio.

The spheroids are centered at the points $x_n = hn$, where n is an integer and h is the chain period. The surface-to-surface separation of two neighboring spheroids is $\sigma = h - 2b$; we require that $h > 2b$ to avoid geometrical intersection of particles. Note that a stronger condition on the interparticle separation will be imposed below. The smaller semiaxis b is assumed to be on the order of 10 nm, while a can be up to a few times larger. We will see that SPPs propagating in such chains have frequencies ω such that the corresponding wavelength in the host medium, $\lambda = 2\pi c_h/\omega$, is considerably larger than both a and b. Accordingly, we adopt the dipole approximation.

This choice, however, requires an additional justification. While the dipole approximation accuracy for electromagnetically interacting spheroids has not been studied directly, many results are available for spheres. The most basic and frequently considered example is that of two electromagnetically interacting spheres in close proximity of each other.[17,18] In this case, the spatially inhomogeneous fields scattered by the spheres result in the excitation of vector spherical harmonics of all orders, even if the spheres are small compared to the wavelength. More specifically, the electric field inside each sphere can be expanded into the vector spherical harmonics with nonzero coefficients appearing in arbitrarily high orders. In the dipole approximation, only the first-order terms ($l=1$, $m=0$, ± 1) are retained in this expansion. The accuracy of this approximation was found to be dramatically affected by polarization. If the electric field polarization is parallel to the axis connecting the spheres, the dipole approximation starts to deviate from the exact solution when $\sigma \approx 0.5R$, with R being the sphere radius, for both dielectric[17] and conducting[18] spheres. However, if the polarization is perpendicular to the axis, the dipole approximation yields results (i.e., the total dipole moment of the spheres[18]) with a relative error of only 2% even in the case $\sigma = 0$. A careful study[19] of the transversely polarized electromagnetic modes of finite-length linear chains of interacting spheres has revealed that the effect of multipole interaction is to slightly shift and broaden the dipole resonance—an effect hardly observable in most materials due to the spectral line broadening associated with Ohmic losses.

Below, we work in the regime when $\sigma = 2b$ ($h = 4b$). In the case of spheres ($b = R$), one could expect the dipole approximation to be very accurate for such relative separations regardless of polarization. We can, however, apply a more stringent test and compare σ to the larger semiaxis of the spheroid, a. Within the dipole approximation, the physical effect described below is manifest for the following aspect ratios. For transversely polarized SPP, the gap in the first

Brillouin zone of the chain lattice appears when $b/a \lesssim 0.25$ in the case of prolate spheroids, and when $b/a \lesssim 0.35$ in the case of oblate spheroids. For longitudinal SPP polarization, the gap appears when $b/a \lesssim 0.1$ in the case of prolate spheroids, and when $b/a \lesssim 0.25$ in the case of oblate spheroids.

Consider first the transverse polarization. The aspect ratio $b/a = 0.25$ corresponds to $\sigma/a = 0.5$. In the case of two spheres of radius R separated by the surface-to-surface distance $\sigma = 0.5R$, the multipole effects are negligible. In fact, even a smaller aspect ratio of $b/a = 0.15$, which is used in the numerical simulations of transversely polarized wave packets in Sec. V, corresponds to the relative separation $\sigma = 0.3R$. At this separation, the multipole effects can still be safely ignored. In the case of the longitudinal polarization, the aspect ratio, which is required to observe the effect in chains of prolate spheroids, is 0.1, which corresponds to $\sigma = 0.2R$. The multipole effects in this situation are expected to be significant but not dramatic. However, in oblate spheroid chains, the required aspect ratio is 0.25, which corresponds to $\sigma = 0.5R$. At this relative separation, the effects of higher multipoles are noticeable but small, even for the longitudinal polarization.

Finally, a simple physical explanation for the dramatic polarization dependence of the dipole approximation accuracy is available. When the polarization is parallel to a chain of spheres, the sphere surfaces, which are adjacent to the "junctions," are similar to usual capacitors, and acquire large and sign-opposite surface charge densities, which, in turn, results in highly nonuniform strongly enhanced local fields. This causes excitation of very high multipole moments. However, for the case of transverse polarization, the surface charge densities near the junctions are proportional to the geometrical factor $\cos\theta$ (θ being the angle between the polarization vector and the radius vector of a point on the sphere surface) and are small. Obviously, this consideration holds for spheroids as well.

We thus conclude that the use of the dipole approximation is well justified for the purpose of this paper. In the case of transverse SPP polarization, the approximation accuracy is exceedingly good. For the longitudinal polarization, the accuracy can be questioned in prolate spheroid chains but is quite reasonable when oblate spheroids are used. We will report numerical computation of the dispersion curves for both prolate and oblate spheroids, in transverse and longitudinal polarization, and for various aspect ratios of the spheroids (Sec. III, Figs. 1–5). However, direct simulation of wave packet propagation (Sec. V, Figs. 8 and 9) is reported only for the choice of parameters such that the accuracy of the dipole approximation is not in doubt.

In the dipole approximation, each nanoparticle is characterized by a (possibly, tensor) dipole polarizability $\alpha(\omega)$ and radiates as a point dipole. The Cartesian components of the nanoparticle dipole moments d_n are coupled to each other and to the external electric field by the coupled-dipole equation,[8,20–22] which we write here in the frequency domain as

$$d_n = \alpha(\omega)\left[E_n^{\text{ext}} + \sum_{m \neq n} G_k(x_n, x_m) d_m \right]. \tag{2}$$

Here E_n^{ext} is the external field amplitude at the nth site, $k = \omega/c_h$ is the wave number in the host material at the frequency ω and $G_k(x, x')$ is the appropriate element of the frequency domain free-space Green's tensor. In this paper, we consider both the transverse and the longitudinal polarizations of the SPP. In the absence of magnetic polarizability of the nanoparticles (which is assumed), the SPPs with the three orthogonal polarizations are not electromagnetically coupled to each other. Therefore, each polarization can be considered separately and the quantities appearing in Eq. (2) should be understood as follows: d_n and E_n^{ext} are projections of the dipole moments and of the external electric field on the selected polarization axis, $\alpha(\omega)$ is the appropriate scalar element of the polarizability tensor and $G_k(x, x')$ is defined by

$$G_k(x,x') = \begin{cases} \left(\dfrac{k^2}{|x-x'|} + \dfrac{ik}{|x-x'|^2} - \dfrac{1}{|x-x'|^3} \right)\exp(ik|x-x'|), & \text{transverse polarization,} \\[4mm] 2\left(-\dfrac{ik}{|x-x'|^2} + \dfrac{1}{|x-x'|^3} \right)\exp(ik|x-x'|), & \text{longitudinal polarization.} \end{cases} \tag{3}$$

III. DISPERSION RELATIONS

An SPP mode is an excitation that propagates along the chain without an external source. Thus, to find the dispersion relation, we seek a solution to Eq. (2) with zero free term, $E_n^{\text{ext}} = 0$, in the form $d_n \propto \exp(iqx_n)$, where q is in the first Brillouin zone of the lattice, $q \in [-\pi/h, \pi/h]$. Substitution of this ansatz into Eq. (2) yields the equation

$$\alpha^{-1}(\omega) = h^{-3} S(hk, hq), \tag{4}$$

where $S(hk, hq)$ is the dimensionless dipole sum (the dipole self-energy) of the chain defined by

$$S(\xi, \eta) = \begin{cases} 2\xi^3 \sum\limits_{n=1}^{\infty} \left[\dfrac{1}{n\xi} + \dfrac{i}{(n\xi)^2} - \dfrac{1}{(n\xi)^3} \right] \exp(in\xi)\cos(n\eta), & \text{transverse polarization,} \\[4mm] 4\xi^3 \sum\limits_{n=1}^{\infty} \left[-\dfrac{i}{(n\xi)^2} + \dfrac{1}{(n\xi)^3} \right] \exp(in\xi)\cos(n\eta), & \text{longitudinal polarization.} \end{cases} \tag{5}$$

Note that the dipole sum is a function of two dimensionless parameters $\xi = kh$ and $\eta = qh$ but does not depend on the particle shape and material properties.

The dispersion relation, i.e., the mathematical dependence of the SPP frequency $\omega = kc_h$ on its Bloch wave number q, can be obtained by finding all pairs of variables (ω, q) that satisfy Eq. (4). This can give rise to one or more branches of the complex function $\omega(q)$. Generally, purely real pairs (ω, q) that solve Eq. (4) do not exist. One can, however, consider purely real values of q and seek complex frequencies, as was done by Koenderink and Polman.[3] The imaginary part of ω is then interpreted as the SPP decay rate. Alternative approaches include numerical computation of discrete modes in a finite chain[1] and plotting $\text{Im}[\alpha^{-1} - h^{-3}S]^{-1}$ as a function of two variables k and q and visually identifying the points at which this function appears to have a maximum or a saddle point.[4]

In this paper, we are interested in propagation of wave packets, which are excited as superpositions of oscillations with purely real frequencies. Since SPPs propagate without radiative losses, their Bloch wave numbers q are purely real if the chain is made of a nonabsorbing material such as an ideal conductor. However, when Ohmic losses in realistic metal are accounted for, q acquires an imaginary part. In what follows, we use two different approaches to computing the dispersion curve. In Sec. III A, we consider chains made of ideal (lossless) metal and seek purely real solutions $\omega(q)$, as was suggested by Simovski.[2] Numerically, this is accomplished by finding pairs of real variables (ω, q) that satisfy the dispersion equation (4) by the method of bisection. Such purely real solutions exist if the permittivity of metal is taken to be real. Next, in Sec. III A, we consider realistic metals. Here we seek pairs (ω, q) that satisfy the dispersion equation such that ω is purely real but q is complex. Numerically, such pairs are obtained by utilizing the root-finding algorithm implemented in Wolfram's *Mathematica*. For the specific case of silver, we find that both approaches yield the results which are very close quantitatively when the dependence of ω on $\text{Re}(q)$ is considered; the first approach, however, provides no information on SPP attenuation which is governed by $\text{Im}\,q$. In both cases, we seek solutions only in the region $\text{Re}\,q > k = \omega/c_h$; as was discussed in the Sec. I, excitations with $\text{Re}\,q < k$ experience radiative decay in addition to Ohmic losses and are not considered in this paper.

A. Dispersion relations for ideal metal

In this section we assume that q and k are real and view the dipole sum $S(kh, qh)$ as a function of two purely real

variables. As the first step, we write the inverse polarizability in Eq. (4) in the form:[23]

$$\alpha^{-1}(\omega) = \alpha_{\text{LL}}^{-1}(\omega) - 2ik^3/3, \tag{6}$$

where $\alpha_{\text{LL}}(\omega)$ is the Lorenz-Lorentz quasistatic polarizability of nanoparticles and $2ik^3/3 = i(2/3)(\omega/c_h)^3$ is the first nonvanishing radiative correction to the inverse polarizability. The inverse of the Lorenz-Lorentz polarizability is given by

$$\alpha_{\text{LL}}^{-1}(\omega) = \frac{4\pi}{\varepsilon_h v}\left(\nu + \frac{\varepsilon_h}{\varepsilon_m - \varepsilon_h} \right), \tag{7}$$

where ν is the appropriate depolarization factor, v is the spheroid volume, and ε_m and ε_h are the permittivities of the (metallic) spheroids and of the host medium, respectively.[24]

In the case of prolate spheroids, the volume is given by

$$v = \frac{4\pi}{3}ab^2, \tag{8}$$

and the three depolarization factors are ν_1 for polarization along the spheroid axis of symmetry and $\nu_2 = \nu_3 = (1-\nu_1)/2$ for two linearly independent transverse polarizations, where

$$\nu_1 = \frac{1-e^2}{e^2}\left[-1 + \frac{1}{2e}\ln\frac{1+e}{1-e} \right]. \tag{9}$$

Here e is the spheroid eccentricity given by formula (1).

For oblate spheroids, the volume is

$$v = \frac{4\pi}{3}a^2b, \tag{10}$$

and the depolarization factors are $\nu_1 = \nu_2$ for two linearly independent polarizations which are orthogonal to the spheroid axis of symmetry and $\nu_3 = 1 - 2\nu_1$ for the polarization along the axis of symmetry, where

$$\nu_1 = \frac{g(e)}{2e^2}\left[\frac{\pi}{2} - \arctan g(e) \right] - \frac{g^2(e)}{2}, \quad g(e) = \frac{\sqrt{1-e^2}}{e}. \tag{11}$$

While both permittivities ε_m and ε_h have, in general, some frequency dependence, here we neglect the dispersion in the host and assume that $\varepsilon_h = \text{const} > 0$. Then, for nanoparticles made of a lossless material, $\text{Im}(\alpha_{\text{LL}}^{-1}) = 0$. At the same time, if $q > k$, the imaginary part of the dipole sum is[8,25] $\text{Im}[S(kh, qh)] = -2(kh)^3/3$ and, in the region of (k, q) which is of interest to us, $\text{Im}[\alpha^{-1} - h^{-3}S] = 0$. Therefore, the imaginary part of Eq. (4) is satisfied identically and only its real part needs to be considered. We then utilize Eqs. (6) and (7) and arrive at the following dispersion equation:

$$\nu + \mathrm{Re}\left(\frac{\epsilon_h}{\epsilon_m - \epsilon_h}\right) = \epsilon_h \frac{\upsilon}{4\pi h^3}\mathrm{Re}[S(hk, hq)]. \qquad (12)$$

In the case of a lossless metal and a transparent host medium, the real part symbol in the left-hand side of Eq. (12) can be omitted.

Equation (12) allows one to analyze the relation between the spheroid aspect ratio and the dispersive properties of the LPCs. Consider first the SPP polarization which is transverse to the chain. For this polarization, the dependence of the real part of the dipole sum $S(kh, qh)$ on its arguments is illustrated in Fig. 1(a) and the relevant depolarization factor is ν_1 (for both prolate and oblate spheroids). We now notice the following: In the spectral region where the metal experiences anomalous dispersion, the second term in the left-hand side of Eq. (12) is negative, assuming that the host medium is a transparent dielectric. When the aspect ratio b/a is decreased, the depolarization factors ν_1 given by Eqs. (9) or (11), for prolate and oblate spheroids, respectively, both approach zero. As a result, the whole left-hand side in Eq. (12) becomes negative. On the other hand, there are regions in the (k, q) space in which the right-hand side of Eq. (12) is strictly positive. Thus, it can be seen from Fig. 1(a) that $\mathrm{Re}[S(kh, qh)] > 0$ if $qh/\pi \gtrsim 0.5$ and $q > k$. As a result, for sufficiently small ratio b/a, Eq. (12) ceases to have real-valued solutions if $q > q_c^\perp$, where $q_c^\perp$ is the (aspect ratio-dependent) critical value of q specific to the transverse polarization. The interval of Bloch wave numbers $q > q_c^\perp$ corresponds to a gap in the first Brillouin zone of the chain lattice. In this gap, SPPs do not exist. It is important to emphasize that the critical constant $q_c^\perp < \pi/h$ exists only for sufficiently small ratio b/a.

Similar considerations can be applied to the longitudinal SPP polarization, except that the relevant depolarization coefficient is, in this case, ν_3. The dependence of $\mathrm{Re}[S(kh, qh)]$ on its arguments is illustrated in Fig. 1(b). It can be seen that $\mathrm{Re}[S(kh, qh)]$ is strictly positive for $qh/\pi \lesssim 0.4$ and $q > k$. Correspondingly, Eq. (12) ceases to have real-valued solutions for $q < q_c^\parallel$, which defines a gap in the first Brillouin zone of the lattice. Here $q_c^\parallel$ is the critical Bloch wave number for the parallel polarization; as in the case of transverse polarization, $q_c^\parallel$ exists only for sufficiently small aspect ratios and is aspect ratio-dependent. Note that the depolarization factor ν_3 approaches a finite value rather than zero when the aspect ratio is decreased. This limit is 1/2 for prolate and 1 for oblate spheroids. Due to this reason, observation of the gap for longitudinally polarized SPPs requires a smaller aspect ratio. This point will be illustrated below by numerical examples.

We now compute the dispersion curves numerically. To solve Eq. (12), a specific expression for the metal permittivity ε_m is needed. We use here the Drude formula,

$$\epsilon_m = \epsilon_0 - \frac{\omega_p^2}{\omega(\omega + i\gamma)}, \qquad (13)$$

where ϵ_0 is the contribution due to interzone transitions,[26] ω_p is the plasma frequency, and γ is the relaxation constant. In this subsection, we set $\gamma = 0$ to describe a lossless metal (re-

(a)

(b)
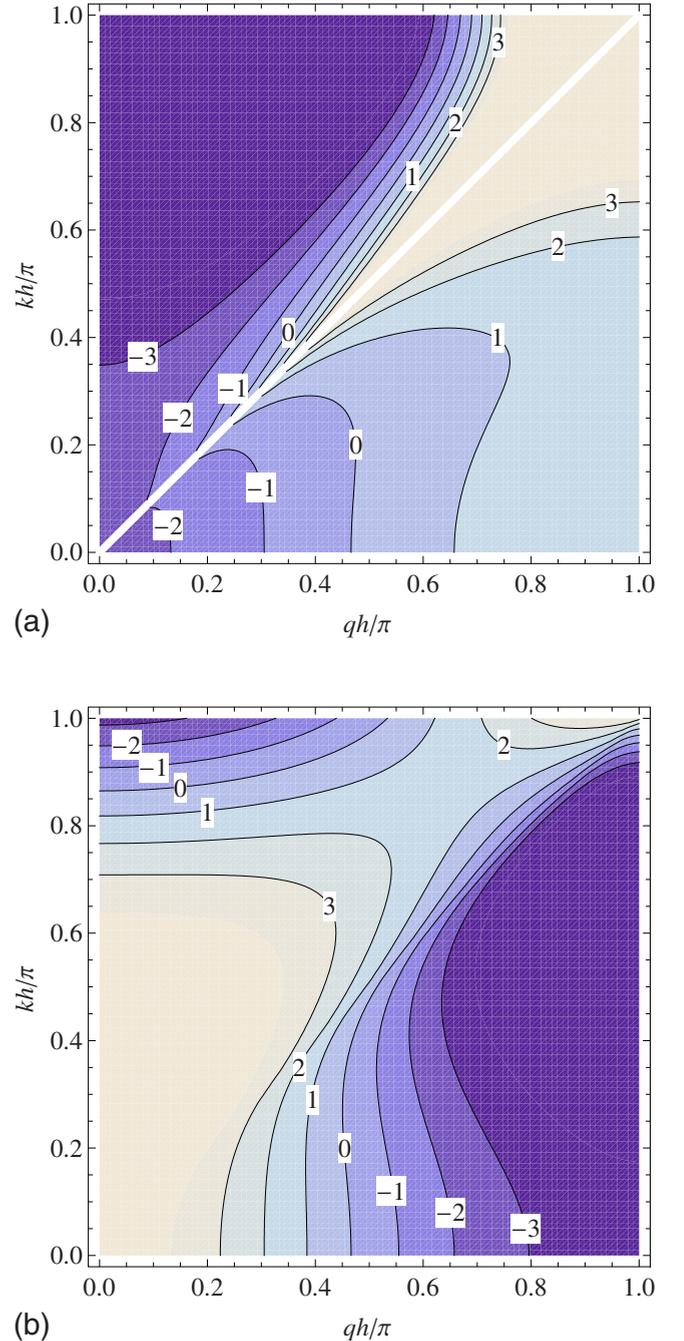
FIG. 1. (Color online) Contour plot of the real part of the dipole sum, $\mathrm{Re}[S(kh, qh)]$ for the transverse (top) and the longitudinal (bottom) polarizations. Due to the symmetry $S(\xi, \eta) = S(\xi, -\eta)$, only the positive half of the first Brillouin zone is shown. Note that, for the transverse polarization, $\mathrm{Re}[S(kh, qh)]$ diverges logarithmically (approaches positive infinity) on the light line $q = k$. Near this line, the function changes so fast that it is not feasible to depict it quantitatively using the contour plot; the region of divergence is schematically shown as a diagonal white line in the top panel. There is no divergence for the longitudinal polarization.

alistic values of γ will be used in Secs. III B and V below). We then solve Eq. (12) by the method of bisection to obtain the dispersion curves and the SPP group velocity.
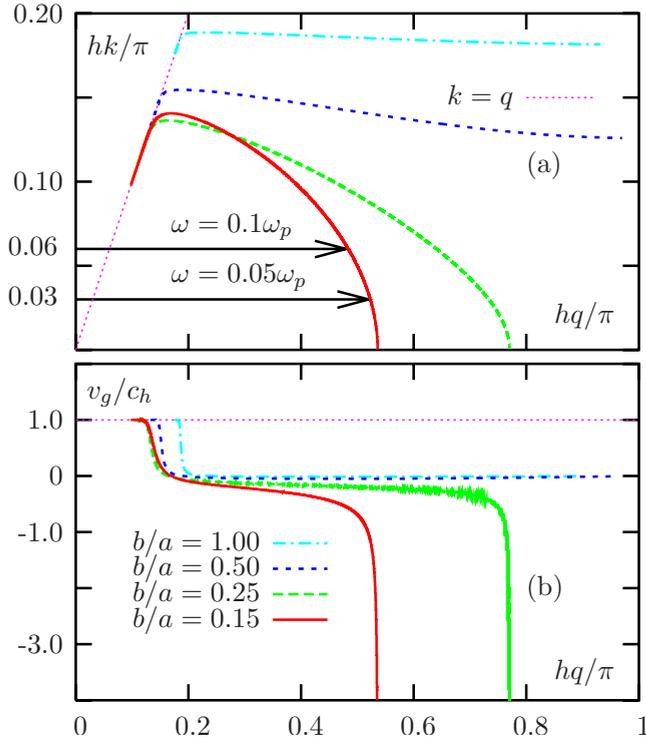
FIG. 2. (Color online) (a) Dispersion curves and (b) group velocity for transversely polarized SPPs in chains built from prolate spheroids whose axis of symmetry is perpendicular to the chain, for different spheroid aspect ratios b/a and for fixed ratios $h/b = 4$ and $\lambda_p/h = 3.4$. Since the dispersion curves are symmetric with respect to the k axis, only the positive half of the first Brillouin zone ($q > 0$) is shown. Only data points that were found numerically are plotted. Theoretically, however, all dispersion curves in infinite chains start at the point $k = q = 0$ and follow the light line (labeled as $k = q$ in the top panel) for some range of q's. Horizontal arrows indicate central frequencies of the Gaussian wave packets whose simulated propagation is illustrated in Fig. 8 below.

The results are shown in Figs. 2–5. The top panels in these four figures show a number of dispersion curves computed for different aspect ratios b/a, as labeled, and for different SPP polarizations. The group velocity of the SPPs, $v_g = \partial\omega/\partial q$, is plotted as a function of q in the bottom panels. The values of ε_h and ε_0 are taken to be 2.5 (as in the case of a glassy medium) and 5.0 (the experimental value for silver[26]), respectively. The computation does not depend on the absolute value of the plasma frequency ω_p but on the dimensionless parameter λ_p/h, where $\lambda_p = 2\pi c_h/\omega_p$ is the wavelength (in the host medium) at the plasma frequency. This ratio was chosen to be $\lambda_p/h = 3.4$. Finally, we have set the ratio $h/b = 4$ so that the minimum surface-to-surface separation of two neighboring spheroids, σ, was equal to $2b$. As an illustration, for the specific case of silver, we have the following parameters: the vacuum plasma wavelength is $\lambda_p^{(vac)} \approx 136$ nm and the corresponding value in the host medium is $\lambda_p = \lambda_p^{(vac)}/\sqrt{\epsilon_h} \approx 86$ nm; correspondingly, $h \approx 25$ nm, $b \approx 6$ nm, and a varies from 6 to 60 nm. The latter value was obtained for the smallest aspect ratio used, $b/a = 0.1$. It can be seen that, for all points on the dispersion curves shown in Figs. 2–5, SPP frequencies are well below
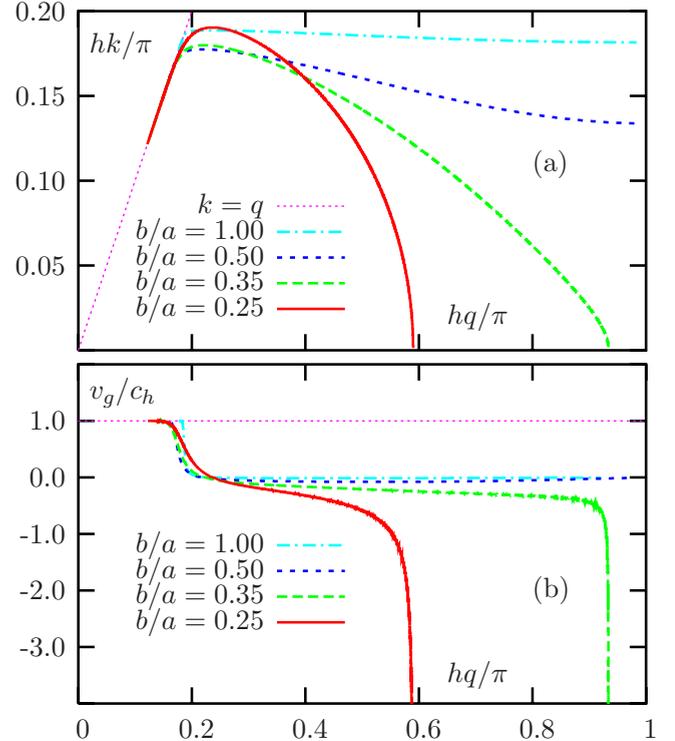
FIG. 3. (Color online) Same as in Fig. 2 but for a chain made of oblate spheroids whose axis of symmetry is parallel to the chain and for a different set of aspect ratios. SPP polarization is orthogonal to the chain.

the plasma frequency ω_p and $kh/\pi \ll 1$. The last inequality is especially strong for the central frequencies (indicated by horizontal arrows in Figs. 2 and 5) which were used to simulate wave packet propagation in Sec. V below. This reconfirms the dipole approximation validity.

We now discuss the computed dispersion curves in more detail, starting with the case of transverse SPP polarization (Figs. 2 and 3). First, we note that in infinite, strictly periodic chains, the dispersion curves of transversely polarized SPPs start at the point $k = q = 0$ and then follow the light line $k = q$ for some range of q. This small-q part of the dispersion curve is related to the logarithmic divergence of the dipole sum on the light line[22] and is extremely difficult to find numerically. Indeed, in order to satisfy Eq. (12), the points on the small-q section of the dispersion curve must be specified with exponentially large numerical precision. This is why the small-q section of the dispersion curve has not been reported in a number of numerical investigations.[1–4] However, the SPPs with $q \approx k \ll \pi/h$ exist and were observed in numerical simulations.[8]

In this paper, we do not consider the small-q part of the dispersion curve but focus on the SPPs for which the ratio k/q is considerably less than unity. Such modes exist for $qh/\pi \gtrsim 0.2$ for all four values of b/a shown in Figs. 2 and 3. The main point of this paper is that the dispersion curve shape is strongly influenced by the ratio b/a. When $b/a = 1.0$, the corresponding dispersion curve is almost flat (apart from the linear small-q section of the curve). At $b/a = 0.5$, the curve begins to bend down noticeably at larger values of q. Finally, when $b/a \lesssim 0.25$ (in the case of prolate spheroids) or
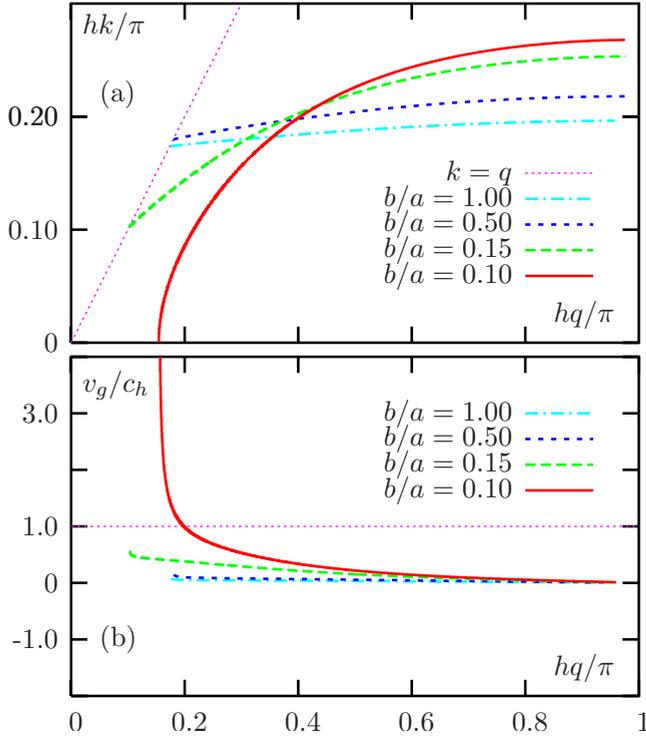
FIG. 4. (Color online) Same as in Fig. 2 but for longitudinal SPP polarization and a different set of aspect ratios. Note that, unlike in the case of transverse polarization, the dispersion curves do not have linear small-q segments. As stated in the text, only data points that satisfy $q \geq k$ are plotted, since there are no real-valued solutions in the region $q < k$.

FIG. 5. (Color online) Same as in Fig. 3 but for longitudinal SPP polarization and a different set of aspect ratios. Note that, unlike in the case of transverse polarization, the dispersion curves do not have linear small-q segments. As stated in the text, only data points that satisfy $q \geq k$ are plotted, since there are no real-valued solutions in the region $q < k$. Horizontal arrows indicate central frequencies of the Gaussian wave packets whose simulated propagation is illustrated in Fig. 9 below.

when $b/a \lesssim 0.35$ (in the case of oblate spheroids), the curves cross the $k=0$ axis at the point $q=q_c^\perp$ and no solutions exist for $q > q_c^\perp$. Near the critical point, the dispersion curves acquires a very large negative slope. Note that the corresponding slope is positive in the $q < 0$ part of the first Brillouin zone (which is not shown in the figures).

From comparison of Figs. 2 and 3, a conclusion can be made that the dispersion curves are more sensitive to the aspect ratio in the case of oblate spheroids. In particular, the gap in the first Brillouin zone of the chain lattice appears for more moderate values of b/a if the chain is made of oblate spheroids.

Dispersion curves for the longitudinal SPP polarization are shown in Figs. 4 and 5. It can be seen that, for sufficiently small aspect ratios, there exists a critical value $q_c^\parallel$ such that Eq. (12) has no real-valued solutions for $q < q_c^\parallel$. Thus, SPP propagation in the chain is only possible for q larger than the critical value $q_c^\parallel$ (if the latter exists). The group velocity shown in Figs. 4(b) and 5(b) acquires large positive values in the vicinity of $q_c^\parallel$.

Similarly to the case of transverse SPP polarization, the dispersion curves are more sensitive to the aspect ratio if the chains are made of oblate spheroids. Thus, in the case of prolate spheroids, the gap in the first Brillouin zone of the lattice appears only when $b/a \lesssim 0.1$. However, if the chain is composed of oblate spheroids, the gap appears when $b/a \lesssim 0.25$.

B. Dispersion relations for realistic metal

The dispersion curves shown in Fig. 2 through Fig. 5 contain no information on either the rate or the direction of SPP spatial decay. However, it can be seen in these figures that an SPP is characterized by phase and group velocities and that these can have different signs when projected onto the x axis. On physical grounds, we expect that wave packets should decay in the direction of propagation. This imposes certain restrictions on the signs of the real and the imaginary parts of q. Thus, if $v_g v_p < 0$, we expect that $\mathrm{Re}(q)\mathrm{Im}(q) < 0$, while if $v_g v_p > 0$, we expect that $\mathrm{Re}(q)\mathrm{Im}(q) > 0$.

The above statement can be illustrated by considering the following thought experiment: Assume that a short Gaussian optical pulse is injected into the central part of a long chain by a spatially localized source such as a near-field microscope tip operating in the illumination mode. The pulse will propagate in the form of two wave packets in both directions along the chain. If $v_g v_p < 0$, both wave packets would be composed of Bloch waves whose phase velocities point toward the source and group velocities point away from the source. Since the sign of the phase velocity is the same as that of $\mathrm{Re}(q)$, and since both wave packets should decay in the direction of propagation, we expect in this case that $\mathrm{Re}(q)\mathrm{Im}(q) < 0$. Similar consideration can be applied to the case $v_g v_p > 0$.
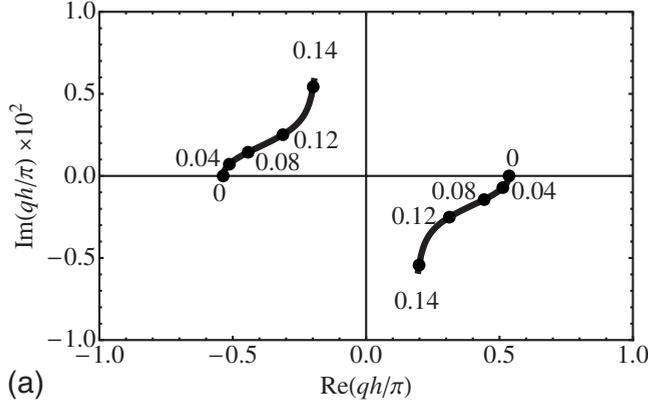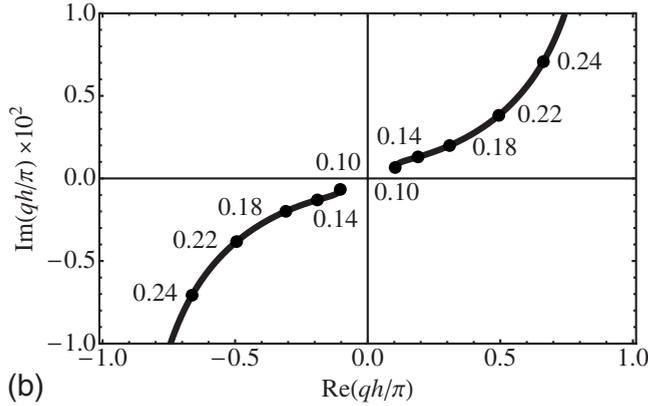
FIG. 6. Dispersion curves plotted parametrically in the complex q plane for (a) transversely and (b) longitudinally polarized SPPs in an LPC of prolate spheroids. Parameters: $\gamma/\omega_p=0.002$, $b/a=0.15$, and other parameters same as in Fig. 2. Dots label the values of the dimensionless parameter $kh/\pi=\omega h/\pi c_h$. In panel (a), only the points in the region $v_p v_g < 0$ are shown, which corresponds, approximately, to $|\text{Re}(q)|h/\pi \gtrsim 0.17$.

In the numerical simulations of this subsection, we have verified that the above analysis is, indeed, correct. To this end, we have incorporated the Ohmic losses into the model of metal permittivity. Specifically, we have set the Drude relaxation constant in Eq. (13) to be $\gamma=0.002\omega_p$ which is the experimental value for silver. Note that Eq. (12) can still be satisfied in this case with a purely real pair of (ω,q) (the real part symbol in the left-hand side of the equation must be retained if ε_m is complex-valued). However, the imaginary part of the more general Eq. (4) is no longer satisfied identically. We, therefore, must seek such pairs of variables (ω,q), where q is now complex, that satisfy both the real and the imaginary parts of Eq. (4). This cannot be achieved by the use of the simple bisection algorithm that was employed in the previous subsection. Instead, we employ here the Wolfram's Mathematica root finder to obtain complex roots of Eq. (4), q, for each real value of ω.

The results of this simulation are plotted parametrically in the complex q plane in Fig. 6 for a chain of prolate spheroids of the aspect ratio $b/a=0.15$ and in Fig. 7 for a chain of oblate spheroids of the aspect ratio $b/a=0.25$. Other parameters are the same as in Fig. 2. As expected, the real and
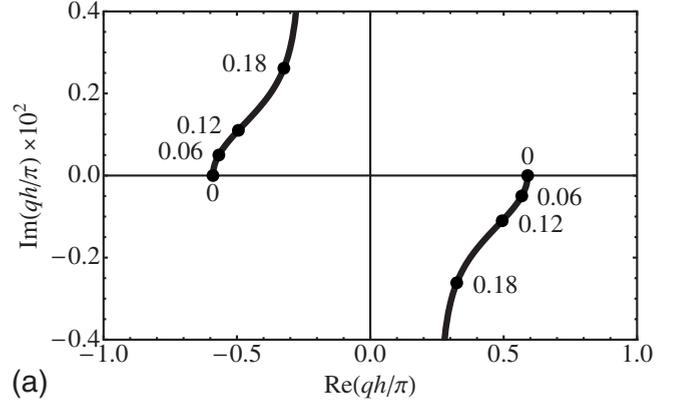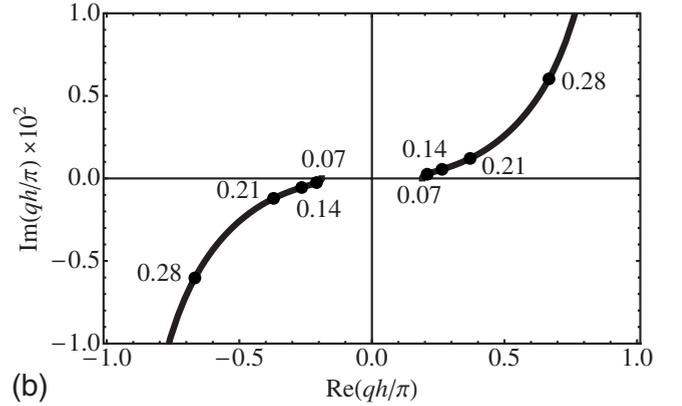
FIG. 7. Same as in Fig. 6 for an LPC of oblate spheroids whose aspect ratio is $b/a=0.25$

imaginary parts of the Bloch wave number have opposite signs for the transversely polarized SPPs so that the wave packets decay in the direction of propagation specified by v_g, even though the phase velocity is pointing into the opposite direction. For longitudinally polarized SPPs the product $v_p v_g$ is always positive and, correspondingly, $\text{Im}(q)\text{Re}(q)>0$.

An important observation is that when $\text{Re}\,q$ approaches one of its critical values, $\text{Im}\,q$ tends to zero. Correspondingly, the decay length of the SPPs is dramatically increased.

We note that the data shown in Fig. 6 represent essentially the same dispersion curves as the ones plotted in Figs. 2(a) and 4(a) for the case $b/a=0.15$. Similarly, data in Fig. 7 correspond to the dispersion curves plotted in Figs. 3(a) and 5(a) for $b/a=0.25$. The discrepancy between the curves $\omega[\text{Re}(q)]$ computed by the two methods is negligibly small. This further justifies the utility of the simple numerical method of Sec. III A for computing the dispersion curves in LPCs.

IV. ATTENUATION OF SPPS AND DECAY LENGTH

The nonzero relaxation constant in Eq. (13) leads to exponential decay of SPPs even in the absence of radiative losses. The decay lengths in LPCs is given by $\ell_{\text{LPC}} = 1/\text{Im}(q)$. If q is not very close to the edge of one of the gaps that were discussed above, ℓ_{LPC} can be computed in the

quasiparticle pole approximation[8] which results in the following expression:

$$\ell_{\text{LPC}} \approx \frac{1}{-h^2 \, \text{Im}[\alpha_{\text{LL}}^{-1}(\omega)]} \left| \frac{\partial \, \text{Re} \, S(\xi, \eta)}{\partial \eta} \right|_{\eta = q_0(\xi)h} \quad (14)$$

where $S(\xi, \eta)$ is the dipole sum given by Eq. (5) and $q_0(\xi)$ is a purely real solution to Eq. (12) for a given value of the dimensionless parameter $\xi = \omega h / c_h$. Under the assumptions that $\epsilon_h, \text{Im}(\epsilon_m) \ll \text{Re}(\epsilon_m)$, we have

$$-\text{Im}[\alpha_{\text{LL}}^{-1}(\omega)] \approx 4\pi\omega\gamma/v\omega_p^2. \quad (15)$$

As we have seen above, the real-valued solutions to Eq. (12) satisfy, albeit approximately, the more general dispersion equation (4). Therefore, we can evaluate the derivative in Eq. (14) at the point (ξ, η) with the understanding that ξ and η are purely real variables that satisfy the approximate dispersion equation (12). We further neglect the terms that are of the order of $\sim 1/\xi$ and $\sim 1/\xi^2$ in the square brackets of the expression (5) for the dipole sum and arrive at the following estimate:

$$\ell_{\text{LPC}} \simeq h \frac{Av}{2\pi h^3} \frac{\omega_p^2}{\omega\gamma} \left| \sum_{m=1}^{\infty} \frac{\cos(\omega h m / c_h)\sin(qhm)}{m^2} \right|, \quad (16)$$

where $A = 1$ for the transverse polarization and $A = 2$ for the longitudinal polarization.

A direct calculation for the transversely polarized SPP in a prolate spheroid chain, $b/a = 0.15$ and other parameters same as in Fig. 2 yields the decay lengths $\ell_{\text{LPC}} \simeq 7$ μm for $\omega = 0.1\omega_p$ and $\ell_{\text{LPC}} \simeq 15$ μm for $\omega = 0.05\omega_p$. Interestingly, the polarization dependence of decay length is contained solely in the factor A. However, the two polarizations have markedly different dispersion curves and therefore same pairs of variables (ξ, η) may not be accessible for the two different polarizations.

It is instructive to compare the SPP decay length in nanoparticle chains and metallic nanowires. The dispersion equation in a metallic cylindrical waveguide is:[27,28]

$$\frac{\epsilon_m I_1(\kappa_m R)}{\kappa_m I_0(\kappa_m R)} + \frac{\epsilon_h K_1(\kappa_h R)}{\kappa_h K_0(\kappa_h R)} = 0, \quad (17)$$

where R is the cylinder radius, $I_l(x)$ and $K_l(x)$ are the modified Bessel functions, $\kappa_{m,h} = \sqrt{q^2 - \epsilon_{m,h}\omega^2/c_h^2}$, and the indices "$m$" and "$h$" label the quantities for the metal and for the surrounding dielectric host, respectively. If the wire is sufficiently thin, we can expand the Bessel function to the first nonvanishing order in $\kappa_m R$ and $\kappa_h R$ to obtain the simplified dispersion equation

$$\epsilon_m = \frac{2\epsilon_h}{(\kappa_h R)^2} \frac{1}{\ln(\kappa_h R/2) + C}, \quad (18)$$

where C is the Euler constant. This equation can be solved approximately (with logarithmic precision) as

$$(\kappa_h R)^2 \approx \frac{2\epsilon_h}{-\epsilon_m} \frac{1}{\frac{1}{2}\ln\dfrac{-2\epsilon_m}{\epsilon_h} - C}. \quad (19)$$

We then use the Drude formula for ϵ_m, take into account the fact that the propagation constant $\text{Re} \, q$ in a metal nanowire is much larger than $\sqrt{\epsilon_h}\omega/c$ (which is the wave number in the surrounding medium), and obtain the following estimate for the decay length:

$$\ell_{\text{wire}} \sim \frac{\omega_p}{\gamma} \frac{R}{2\sqrt{2\epsilon_h}}, \quad (20)$$

One additional condition that has been used in deriving the above estimate is $\omega \gg \gamma$. For a silver nanowire of radius $R = 25$ nm, the estimate yields $\ell_{\text{wire}} \approx 2.8$ μm.

The following conclusions can be made: While the SPP decay length in nanowires depends only on the metal and host permittivities and the waveguide radius, the same quantity in the LPCs can be controlled by changing the interparticle separation and the particle dimensions. Decreasing the interparticle spacings results in stronger electromagnetic coupling and larger propagation distances. However, for sufficiently small values of h, the dipole approximation breaks down and the estimate [Eq. (16)] becomes invalid. The dimensions of a nanoparticle provide another set of degrees of freedom in controlling the decay length in LPCs. Note that the expression (16) contains an overall factor $v/2\pi h^3$, which can be interpreted as the volume fraction of metal (in a unit cell of the chain lattice). For an LPC of prolate spheroids, this factor is equal to $2ab^2/3h^3$. However, for an LPC made of oblate spheroids, the factor is $2a^2b/3h^3$. It obtains that the propagation distance in oblate spheroid LPCs is effectively increased by the factor of $a/b > 1$ compared to prolate spheroid LPCs. Thus constructing an LPC from thin nanodisks whose axis of symmetry is parallel to the chain axis may be beneficial.

V. MODELING OF WAVE PACKET PROPAGATION

We now demonstrate that superluminal wave packets can indeed propagate in chains with sufficiently small aspect ratios b/a. To this end, we consider a finite chain of N nanoparticles excited by a pulse with Gaussian temporal profile incident on the first particle in the chain. In the time domain, the pulse is described by the formula

$$E_n^{\text{ext}}(t) = \delta_{n1}\mathcal{E}\exp[-i\omega_0 t - (t/\Delta t)^2], \quad (21)$$

where $\mathcal{E}$ is an arbitrary amplitude and Δt is the pulse duration. This function has the Fourier transform

$$\widetilde{E}_n^{\text{ext}}(\omega) = \delta_{n1}\sqrt{\pi}\Delta t\mathcal{E}\exp\left[-\frac{(\omega - \omega_0)^2}{(\Delta\omega)^2}\right], \quad \Delta\omega = \frac{2}{\Delta t}. \quad (22)$$

The numerical procedure is as follows: The above expression for $\widetilde{E}_n^{\text{ext}}(\omega)$ is used as the free term in the right-hand side of Eq. (2). The equation is solved numerically by direct matrix inversion for multiple values of ω sampled in a sufficiently
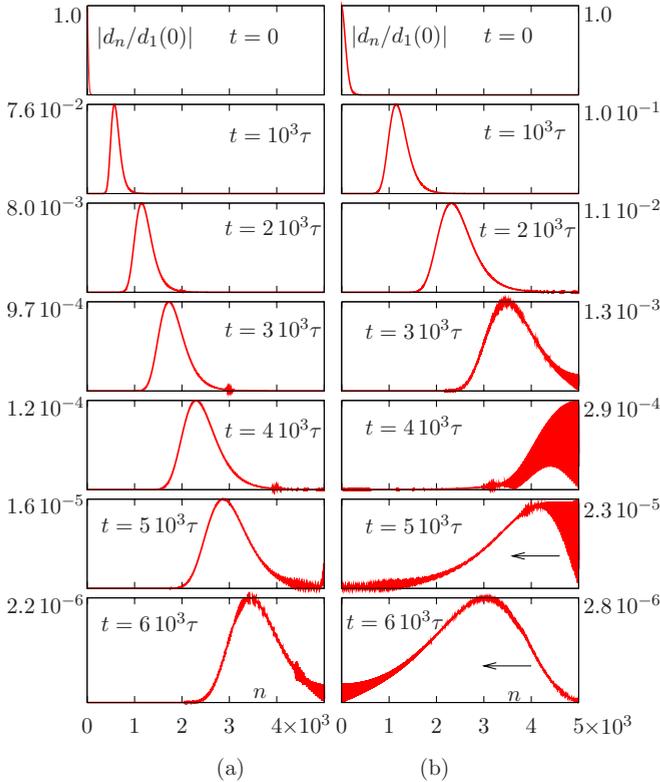
FIG. 8. (Color online) Envelopes of transversely polarized wave packets in a chain of $N=5000$ prolate nanospheroids with the aspect ratio $b/a=0.15$ at different moments of time t. Spheroids are oriented so that their axes of symmetry are perpendicular to the chain axis. Time is measured in the units of $\tau=h/c_h$. Column (a): $\omega_0 =0.1\omega_p$ and $v_g \approx 0.57c_h$. Column (b): $\omega_0=0.05\omega_p$ and $v_g \approx 1.16c_h$. Arrows indicate that the wave packet propagates from right to left after being reflected from the far end of the chain.

FIG. 9. (Color online) Envelopes of longitudinally polarized wave packets in a chain of $N=5000$ oblate nanospheroids with the aspect ratio $b/a=0.25$ at different moments of time t. Spheroids are oriented so that their axes of symmetry coincide with the chain axis. Time is measured in the units of $\tau=h/c_h$. Note that the largest time shown in this figure is two times smaller than the respective quantity in Fig. 8. Column (a): $\omega_0=0.25\omega_p$ and $v_g \approx 0.77c_h$. Column (b): $\omega_0=0.10\omega_p$ and $v_g \approx 2.57c_h$. Arrows indicate that the wave packet propagates from right to left after being reflected from the far end of the chain.

large interval and with sufficiently small step to ensure convergence. This yields a family of numerical solutions $\tilde{d}_n(\omega)$. The real time quantities $d_n(t)$ are then obtained by the inverse Fourier transform according to

$$d_n(t) = \int \tilde{d}_n(\omega)\exp(-i\omega t)\frac{d\omega}{2\pi}. \tag{23}$$

Numerically, this integral is evaluated by the trapezoidal rule.

We have simulated transversely polarized wave packets in LPCs of prolate spheroids with the aspect ratio $b/a=0.15$. Longitudinally polarized SPPs were simulated in chains of oblate spheroids with the aspect ratio $b/a=0.25$. Simulations were performed in a chain consisting of $N=5\cdot10^3$ spheroids; the overall length of the chain was (given $h=25$ nm) $L =125$ μm. All parameters were the same as those used for calculating dispersion curves shown in Fig. 2, with the only exception that Ohmic losses in the metal were taken into account by means of using the nonzero Drude relaxation constant $\gamma=0.002\omega_p$. Four sets of simulations have been performed, the first two for the transverse and the other two for the longitudinal polarization.

In the case of the transverse polarization, two different central frequencies of the pulse have been used. The first pulse had the central frequency $\omega_0=0.1\omega_p$ (correspondingly, $k_0h/\pi=0.06$ where $k_0=\omega_0/c_h$) and the pulse spectral width was $\Delta\omega=\omega_0/5$. Thus the excitation was relatively broadband but very narrow in the time domain: given the experimental value of ω_p for silver, the above spectral width corresponds to $\Delta t \approx 7.2$ fsec. The second pulse had the central frequency twice smaller than the first, $\omega_0=0.05\omega_p$, with the same relative spectral width $\Delta\omega=\omega_0/5$. In the time domain, this corresponds to $\Delta t \approx 14.2$ fsec. The central frequencies of the two pulses are shown in Fig. 2(a) by the horizontal arrows. Amplitudes of the obtained wave packets are illustrated in Fig. 8 at different moments of time measured in the units of $\tau=h/c_h$. The maximum time shown on the plots is $t=6\times10^3\tau\approx800$ fsec.

It can be seen that the wave packet with $\omega_0=0.1\omega_p$ propagates away from the source with the subluminal group velocity $v_g \approx 0.57c_h$. However, the wave packet with the smaller central frequency propagates at the speed $v_g \approx 1.16c_h$. These group velocities are in quantitative agreement with the data shown in Fig. 2(b). Note that the group velocities can be evaluated as the slopes of the dispersion

curve drawn for $b/a=0.15$ in Fig. 2(a) at the central frequencies indicated by the horizontal arrows. As expected, the superluminal wave packet is spreading faster than the subluminal wave packet. This is so because of the larger value of the second derivative $\partial^2\omega/\partial^2 q$ at the smaller central frequency. Yet, near the end of the chain, the duration of the superluminal pulse is still only ≈ 1 psec.

The two sets of simulations for the longitudinal polarization are shown in Fig. 9. Here we have used a chain of oblate spheroids with the aspect ratio $b/a=0.25$. The central frequencies of the two pulses were $\omega_0=0.25\omega_p$ and $\omega_0=0.1\omega_p$. The pulses' relative spectral widths were the same as in the case of the transverse polarization, namely, the pulse spectral width was $\Delta\omega=\omega_0/5$. By tracing the maximum of each wave packet, we deduce $v_g\approx 0.88c_h$ for $\omega_0=0.25\omega_p$ and $v_g \approx 2.17c_h$ for $\omega_0=0.1\omega_p$. This is in full agreement with the group velocities shown in Fig. 5(b).

Finally, note that the decay lengths in each simulation cannot be easily deduced from the time evolution of the maxima of the wave packets. This is because the propagation is accompanied by both decay and spreading. The latter takes place even in the absence of Ohmic losses.

VI. CONCLUDING REMARKS

In this paper, we have employed the coupled dipole approximation to compute the dispersion curves and to model propagation of wave packets of surface plasmon polaritons (SPPs) in linear periodic chains (LPCs) of metallic nanospheroids.

We have shown that the group velocity, the decay length, and the bandwidth of SPPs propagating in LPCs of metallic nanoparticles can be effectively tuned. The tunability is achieved by means of varying the nanoparticles aspect ratio. The decay length can be dramatically increased for Bloch wave numbers q near the edges of gaps that appear in the first Brillouin zone of the lattice for sufficiently small aspect ratios. At the same time, the SPP group velocity is increased up to superluminal values. By replacing the host medium with vacuum, it is also possible to excite a wave packet whose group velocity is larger than the speed of light in vacuum. Such wave packets exist in nature and were observed experimentally.[14,15]

Comparison of Figs. 2–5 reveals that the parameters of two different LPCs can be tuned so that one LPC supports transversely polarized SPPs and the other chain supports longitudinally polarized SPPs with *the same electromagnetic frequency*. This fact can be utilized for guiding the SPPs through corners (ninety degree turn in an LPC) and/or for splitting and coupling the SPPs at T junctions. Another potentially interesting element of an integrated photonic circuit a two-segment straight LPC. Assume that, at a given frequency, one segment can support only transversely polarized SPPs while the other segment supports only longitudinally polarized SPPs. At the junction of the two segments, an externally manipulated (i.e., by magnetic field) coupling nanospheroid is placed. When the coupling nanospheroid makes the angle of either 0 or π with respect to the chain axis, the two segments are decoupled and do not allow direct trans-

mission of light pulses. However, if the coupling spheroid is rotated by the angle of $\pi/4$ with respect to the axis, the transversely polarized SPP propagating in the first segment is coupled to the longitudinally polarized SPP in the second segment and transmission along the chain becomes possible. Detailed investigation of these possibilities will be the subject of future work.

In the case of transverse SPP polarization, the group and phase velocities of SPPs can be antiparallel. We, however, have found that the negative group velocity *per se* (defined here by the condition $v_g v_p < 0$) does not necessarily imply superluminal propagation or a negative time delay as was suggested previously.[13,29] For example, the wave packet shown in Fig. 8(a) propagates slower than c_h even though it is composed of waves whose frequencies are in the negative dispersion region. It is important to realize that the effects theoretically described in these two references, as well as the corresponding experimental observations,[14,15] involve propagation of an optical pulse from a medium with normal dispersion to a medium with negative dispersion and the presence of the interface is essential. In this paper, we are looking at a somewhat different physical situation when the optical pulse is injected into a waveguide by a predetermined external source, which is located in the near field of the waveguide. We then observe that the pulse propagates away from the source with the velocity $|v_g|$, irrespectively of the sign of the product $v_g v_p$. Thus the superluminal propagation is obtained when $|v_g|>c_h$ but not necessarily when $v_g v_p < 0$.

Antiparallel phase and group velocities that we have observed in the case of transverse SPP polarization deserve a separate discussion. We believe that this phenomenon cannot be interpreted as "negative refraction." The reason is that the LPCs considered in this paper are essentially discrete objects and cannot be described by effective medium parameters. The elementary excitations that propagate in LPCs are Bloch waves rather than sinusoidal waves, and this fact should not be disregarded. The region of negative dispersion shown in Fig. 2(a) starts at $qh\approx 0.2\pi\approx 0.6$. In general, the chain can be viewed as continuous only when $qh\ll 1$. The above condition is not satisfied in the region of negative dispersion. It is, however, not clear *a priori*, how strong this inequality should be for the effective medium approximation to be valid. In the specific case of LPCs, one can consider the following argument: We expect the effective medium parameters such as the permittivity $\varepsilon(\omega)$ or the refraction index $n(\omega)$ to be single-valued functions of their argument. However, for every point on the negative slope section of the dispersion curves shown in Fig. 2(a), there is another point on the same curve with the same frequency but a smaller value of q. This second point is located on the linear small-q section of the dispersion curve. Although this small-q section is difficult to find numerically (and, as a result, is often overlooked), it exists. It is therefore logical to assume that, if a chain be assigned some effective medium parameter for a given frequency ω, this parameter must be computed using the point on the small-q section of the dispersion curve. The

latter exhibits positive (and linear) dispersion. In the above argument, we have disregarded the possibility of introducing nonlocal effective medium parameters, which are character-istic, for example, of chiral media and can result in negative dispersion.[30] However, the physical object that we consider in this paper is essentially nonchiral.

*algov@seas.upenn.edu

†vmarkel@mail.med.upenn.edu.

[1] W. H. Weber and G. W. Ford, Phys. Rev. B **70**, 125429 (2004).

[2] C. R. Simovski, A. J. Viitanen, and S. A. Tretyakov, Phys. Rev. E **72**, 066606 (2005).

[3] A. F. Koenderink and A. Polman, Phys. Rev. B **74**, 033402 (2006).

[4] K. H. Fung and C. T. Chan, Opt. Lett. **32**, 973 (2007).

[5] S. Y. Park and D. Stroud, Phys. Rev. B **69**, 125418 (2004).

[6] D. S. Citrin, Nano Lett. **5**, 985 (2005).

[7] D. S. Citrin, Opt. Lett. **31**, 98 (2006).

[8] V. A. Markel and A. K. Sarychev, Phys. Rev. B **75**, 085426 (2007).

[9] M. Quinten, A. Leitner, J. R. Krenn, and F. R. Ausennegg, Opt. Lett. **23**, 1331 (1998).

[10] M. L. Brongersma, J. W. Hartman, and H. A. Atwater, Phys. Rev. B **62**, R16356 (2000).

[11] S. A. Maier, P. G. Kik, H. A. Atwater, S. Meltzer, E. Harel, B. E. Koel, and A. G. Requicha, Nat. Mater. **2**, 229 (2003).

[12] S. A. Maier, P. G. Kik, and H. A. Atwater, Appl. Phys. Lett. **81**, 1714 (2002).

[13] E. L. Bolda, J. C. Garrison, and R. Y. Chiao, Phys. Rev. A **49**, 2938 (1994).

[14] L. J. Wang, A. Kuzmich, and A. Dogariu, Nature (London) **406**, 277 (2000).

[15] G. M. Gehring, A. Schweinsberg, C. Barsi, N. Kostinski, and R. W. Boyd, Science **312**, 895 (2006).

[16] A. F. Koenderink, R. deWaele, J. C. Prangsma, and A. Polman, Phys. Rev. B **76**, 201403(R) (2007).

[17] R. Ruppin, J. Phys. Soc. Jpn. **58**, 1446 (1989).

[18] I. E. Mazets, Tech. Phys. **45**, 1238 (2000).

[19] V. A. Markel, V. N. Pustovit, S. V. Karpov, A. V. Obuschenko, V. S. Gerasimov, and I. L. Isaev, Phys. Rev. B **70**, 054202 (2004).

[20] V. A. Markel, J. Mod. Opt. **40**, 2281 (1993).

[21] V. A. Markel, J. Opt. Soc. Am. B **12**, 1783 (1995).

[22] V. A. Markel, J. Phys. B **38**, L115 (2005).

[23] V. A. Markel, J. Mod. Opt. **39**, 853 (1992).

[24] C. F. Bohren and D. R. Huffman, *Absorption and Scattering of Light by Small Particles* (Wiley, New York, 1983).

[25] A. L. Burin, H. Cao, G. C. Schatz, and M. A. Ratner, J. Opt. Soc. Am. B **21**, 121 (2004).

[26] U. Kreibig and L. Genzel, Surf. Sci. **156**, 678 (1985).

[27] A. A. Govyadinov and V. A. Podolskiy, Phys. Rev. Lett. **97**, 223902 (2006).

[28] D. E. Chang, A. S. Sorensen, P. R. Hemmer, and M. D. Lukin, Phys. Rev. B **76**, 035420 (2007).

[29] A. Dogariu, A. Kuzmich, and L. J. Wang, Phys. Rev. A **63**, 053806 (2001).

[30] V. M. Agranovich, Y. N. Gartstein, and A. A. Zakhidov, Phys. Rev. B **73**, 045114 (2006).